

New insights into defibrillation of the heart from realistic simulation studies

Natalia A. Trayanova^{1,2*} and Lukas J. Rantner^{1,2}

¹Department of Biomedical Engineering, Johns Hopkins University School of Medicine, 3400 N Charles Street, 216 Hackerman Hall, Baltimore, MD 21218, USA; and

²Institute for Computational Medicine, Johns Hopkins University, 3400 N Charles Street, Baltimore, MD 21218, USA

Received 31 May 2013; accepted after revision 17 September 2013

Cardiac defibrillation, as accomplished nowadays by automatic, implantable devices, constitutes the most important means of combating sudden cardiac death. Advancing our understanding towards a full appreciation of the mechanisms by which a shock interacts with the heart, particularly under diseased conditions, is a promising approach to achieve an optimal therapy. The aim of this article is to assess the current state-of-the-art in whole-heart defibrillation modelling, focusing on major insights that have been obtained using defibrillation models, primarily those of realistic heart geometry and disease remodelling. The article showcases the contributions that modelling and simulation have made to our understanding of the defibrillation process. The review thus provides an example of biophysically based computational modelling of the heart (i.e. cardiac defibrillation) that has advanced the understanding of cardiac electrophysiological interaction at the organ level, and has the potential to contribute to the betterment of the clinical practice of defibrillation.

Keywords

Computer simulation • Electric countershock • Ventricular fibrillation

Introduction

Cardiac fibrillation is the breakdown of the organized cardiac electrical activity driving the heart's periodic pumping, into disorganized self-sustained electrical activation patterns. A fibrillation episode results in the loss of cardiac output, and unless timely intervention is administered, death quickly ensues. The only known effective therapy for lethal disturbances in cardiac rhythm is defibrillation, the delivery of a strong electric shock to the heart. This technique, as accomplished nowadays by automatic, implantable devices, constitutes the most important means of combating sudden cardiac death. However, uncovering how electric current delivered to the heart to terminate lethal arrhythmias traverses myocardial structures and interacts with the wavefronts of fibrillation has proven enormously challenging. Of particular importance has been to obtain insight into the mechanisms by which the high-voltage shock fails, since re-initiation of fibrillation is related not only to the effect of the shock on the electrical state of the myocardium, but also to the intrinsic properties of the tissue that lead to de-stabilization of post-shock activations and their degradation into electric turbulence. Realistic three-dimensional (3D) simulations of the ventricular defibrillation process in close conjunction with experimental observations have proven to be an invaluable tool in the pursuit to understand the electrical events that ensue from the interaction between fibrillating

myocardium and applied shock. The goal of this review article is to present an overview of the contributions made by such models. Particular emphasis is given to models of defibrillation in the diseased heart.

Experimental approaches to investigate high-voltage defibrillation mechanisms

The key to understanding the cardiac defibrillation process is to uncover those mechanisms by which electric current delivered to the heart by the shock traverses myocardial structures and interacts with the wavefronts of fibrillation. Early studies on defibrillation mechanisms relied on recordings of extracellular potentials following the defibrillation shock, since overwhelming electrical artefacts had prevented researchers from recording during and shortly after the shock. Although these pioneering electrical mapping studies provided insights that laid the basis for understanding defibrillation mechanisms, such as the upper limit of vulnerability (ULV), there was no direct experimental evidence to prove the putative mechanisms. A major breakthrough occurred with the introduction of potentiometric dyes, which allowed recording of electrical events before, during, and after shock delivery with high resolution. The ability of these optical mapping techniques to record optical fluorescence signals proportional to the transmembrane voltage, V_m , proved

* Corresponding author. Tel: +1 410 516 4375; fax: +1 410 516 5294, E-mail address: ntrayanova@jhu.edu

Published on behalf of the European Society of Cardiology. All rights reserved. © The Author 2013. For permissions please email: journals.permissions@oup.com.

to be a major advantage. Unlike extracellularly recorded electric potentials, which integrate contributions of bioelectric activity in the vicinity of a recording site via the volume conductor in which the heart is immersed, recording V_m provides a direct measure of the shock-induced membrane responses. Although optical mapping techniques allow the visualization of shock-induced changes in membrane potential, these recordings are, however, confined to activity on the cardiac surfaces only. In a complex 3D anatomical structure such as the heart, shock-induced electrical events and post-shock activity take place throughout the myocardial walls. Therefore, the restricted capability of current optical mapping techniques to detect events occurring in the depth of the wall that may not have any signature on the surfaces¹ poses a significant limitation.

Computer modelling of the high-voltage defibrillation process: mechanistic insights

Virtual electrode polarization and its role in defibrillation

The absence of experimental methodology for recording shock-induced membrane polarizations in 3D has provided a major impetus for the development and refinement of computer models of the cardiac defibrillation process.^{1–12} Since there is insufficient direct experimental evidence to allow a direct verification of model predictions in the depth of the myocardium, results of computer models are being compared against optical maps recorded on the ventricular surfaces. Assuming that model formulations are a valid, quantitatively correct representation of cardiac bioelectricity, models that correctly predict experimental observations at the surfaces are used to predict behaviour inside the depth of the myocardial walls.^{2,13}

Using the bidomain model of the myocardium, which explicitly accounts for current flow in both the intracellular and the interstitial domains, Sepulveda *et al.*¹⁴ demonstrated in a seminal study that shock-induced changes in membrane potential (membrane polarization) can be much more complex than previously anticipated. Their simulation results suggested that the tissue response in the vicinity of a strong unipolar stimulus involved the simultaneous occurrence of both positive (depolarizing) and negative (hyperpolarizing) effects in close proximity, if the anisotropy ratios between intracellular and extracellular spaces comprising the myocardium are unequal, i.e. both spaces are anisotropic, but to a different degree. In the absence of unequal anisotropy ratios, as it is the case with monodomain models which inherently assume equal anisotropies, no polarizations of opposite polarity can occur.¹⁵ This prediction of the existence of 'virtual electrodes' was followed by optical mapping studies that convincingly confirmed these theoretical predictions.¹⁶ Since, 'virtual electrode polarization' (VEP) has been documented in experiments involving various stimulus configurations,^{9,17–19} and has become a mainstay in defibrillation research. Virtual electrode polarization in the myocardium now refers universally to the regions of membrane depolarization and hyperpolarization induced by an electric shock.^{20,21} Shock-induced membrane depolarization and hyperpolarization and their spatial pattern in the ventricles represent a new state of the myocardium that is established at the end of

the shock; the electrical activity that follows is strongly dependent on this new state.^{3,22,23}

Conceptually, defibrillation can be considered to be a two-step process. First, the applied shock drives currents that traverse the myocardium and cause complex polarization changes in V_m distribution,²⁴ i.e. VEP. Secondly, post-shock active membrane reactions are invoked that eventually result either in termination of fibrillation in the case of shock success, or in re-initiation of fibrillatory activity in the case of shock failure. Using computer models to analyse the aetiology of VEP patterns established by the shock (i.e. the first step of the defibrillation process) revealed that the shape, location, polarity, and intensity of shock-induced VEPs are determined by both the cardiac tissue structure as well as the configuration of the applied field.^{2,18,24–26} Based on theoretical considerations, VEPs can be classified either as 'surface VEP', which penetrates the ventricular wall over a few cell layers, or as 'bulk VEP' where polarizations arise throughout the ventricular wall.^{27,28} Analysis of the bidomain equations revealed that a necessary condition for the existence of the bulk VEP is the presence of unequal anisotropy ratios in the myocardium. Sufficient conditions include either spatial non-uniformity in the applied electric field,¹⁸ or non-uniformity in tissue architecture, such as fibre curvature,²⁹ fibre rotation,²⁸ fibre branching and anastomosis, and local changes in tissue conductivity due to resistive heterogeneities.^{30–32} Figure 1 presents VEPs developed at the end of the defibrillation shock in a realistic model of the rabbit heart under various conditions (shock strengths, durations, waveforms, polarities, and timings of shock delivery).

In the second phase of the defibrillation process, the local cellular response to the shock throughout the myocardium depends on local VEP magnitude and polarity as well as on the local pre-shock state of the tissue. Local action potential duration can be either extended (by positive VEP) or shortened (by negative VEP) to a degree that depends on local VEP magnitude and shock timing, with strong negative VEP completely abolishing (de-exciting) the local action potential, thus creating post-shock excitable gaps. As demonstrated in bidomain modelling studies,^{1,34} the post-shock VEP pattern is also the major determinant of the origin of post-shock activations that develop in the second part of the defibrillation process. In those regions where shock-induced virtual anodes (regions of membrane potential below rest) and cathodes (regions of membrane depolarization) are in close proximity, a 'break' excitation following the end of the shock (i.e. at the 'break' of the shock) can be elicited. The depolarized cells in the virtual cathode serve to provide an electrical stimulus (excitatory current) eliciting a regenerative depolarization and a propagating wave in the newly created excitable area (virtual anodes) located in immediate proximity. Whether or not break excitations arise depends on whether the V_m gradient across the border between a virtual anode and a neighbouring virtual cathode spans the threshold for regenerative depolarization.³⁵ The finding of break excitations, combined with the fact that positive VEP can also result in 'make' excitations³⁶ (straightforward depolarization by the shock of the excitable gaps present at the time of shock delivery, i.e. at 'make' of the shock, in the fibrillating myocardium) in regions where tissue is at or near diastole, resulted in a novel understanding of how a strong stimulus can trigger the development of new activations.

According to VEP theory and the simulation and experimental research supporting it, mechanisms for shock success or failure are

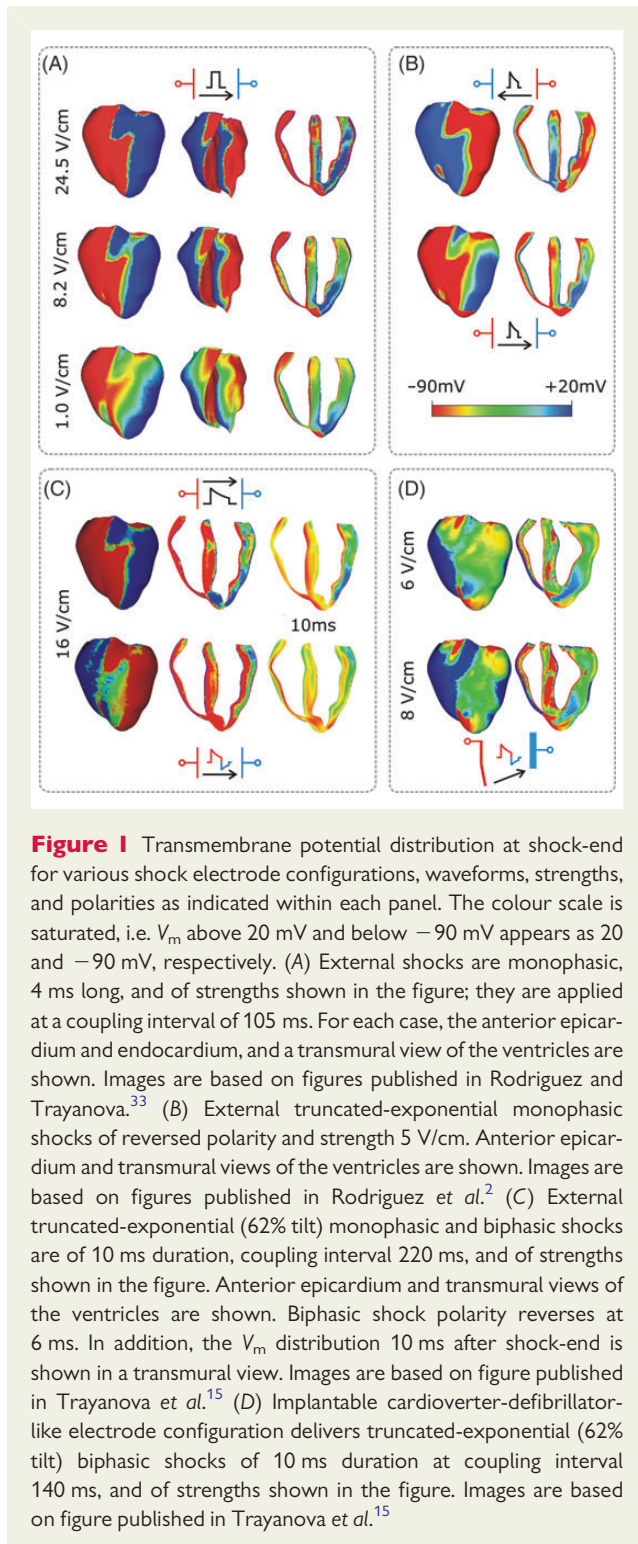


Figure 1 Transmembrane potential distribution at shock-end for various shock electrode configurations, waveforms, strengths, and polarities as indicated within each panel. The colour scale is saturated, i.e. V_m above 20 mV and below -90 mV appears as 20 and -90 mV, respectively. (A) External shocks are monophasic, 4 ms long, and of strengths shown in the figure; they are applied at a coupling interval of 105 ms. For each case, the anterior epicardium and endocardium, and a transmural view of the ventricles are shown. Images are based on figures published in Rodriguez and Trayanova.³³ (B) External truncated-exponential monophasic shocks of reversed polarity and strength 5 V/cm. Anterior epicardium and transmural views of the ventricles are shown. Images are based on figures published in Rodriguez *et al.*² (C) External truncated-exponential (62% tilt) monophasic and biphasic shocks are of 10 ms duration, coupling interval 220 ms, and of strengths shown in the figure. Anterior epicardium and transmural views of the ventricles are shown. Biphasic shock polarity reverses at 6 ms. In addition, the V_m distribution 10 ms after shock-end is shown in a transmural view. Images are based on figure published in Trayanova *et al.*¹⁵ (D) Implantable cardioverter-defibrillator-like electrode configuration delivers truncated-exponential (62% tilt) biphasic shocks of 10 ms duration at coupling interval 140 ms, and of strengths shown in the figure. Images are based on figure published in Trayanova *et al.*¹⁵

multifactorial, depending mainly on the post-shock distribution of V_m as well as timing and speed of propagation of the shock-induced wavefronts. Whether depolarization of the post-shock excitable gap is achieved in time to block its invasion by incoming wavefronts critically depends on (i) the number and conduction velocity of the post-shock 'break' activations that propagate through it to render it refractory, and (ii) on the time interval over which this depolarization

of the excitable gap needs to be achieved, which depends on how fast the surrounding refractory regions recover excitability. All factors depend, ultimately, on shock strength. Increasing shock strength results in higher voltage gradients across borders between regions of opposite polarity, leading to more break excitations³⁵ which then traverse the post-shock excitable gap earlier³⁷ and at a faster velocity,³⁵ as well as extend the refractoriness of the tissue surrounding the excitable gap to a larger degree,³⁸ ultimately resulting in termination of all post-shock wavefronts. Finally, modelling studies^{39,40} have also demonstrated that the complexity of pre-shock activity is an important factor in the outcome of the defibrillation shock. To ascertain the predictive capabilities of the modelling studies described above, simulation results of defibrillation have been compared with optimal mapping results; to do so, the process of optical mapping was successfully modelled.^{13,41}

It is important to note that the mechanisms of cardiac defibrillation have been strongly linked to cardiac vulnerability to electric shocks, i.e. the induction of arrhythmia by electric shocks. An electric shock can induce ventricular arrhythmias if it is given during the vulnerable period within the normal cardiac cycle. Shocks that result in induction of arrhythmia are bound by a maximum strength, termed the ULV.⁴² Studies have found a strong correlation between ULV and the minimum shock strength that results in successful defibrillation, i.e. the defibrillation threshold (DFT).⁴³ Therefore, understanding cardiac vulnerability to electric shocks has traditionally been a route to understanding defibrillation and arrhythmogenesis by failed shocks, a route that will also be emphasized in this review, since many studies have focused on exploring vulnerability to electric shocks as a surrogate to understanding the failure of defibrillation.

The role of shock waveform

The issue of shock waveform has been an important development in the clinical procedure of defibrillation. Reversal of shock polarity during defibrillation, such as in biphasic shock waveforms, has been found to improve defibrillation efficacy, and is the current standard in clinical defibrillation. The mechanisms underlying the superiority of biphasic shock waveforms in achieving defibrillation success has been the subject of a large body of research. Simulation studies and the advancement of the VEP theory for defibrillation have offered new insights into the improved efficacy of biphasic waveforms, but also into the specific mechanisms by which biphasic shocks fail under certain circumstances. Anderson *et al.*⁴⁴ demonstrated that transmembrane potential gradients formed after an optimal biphasic shock could give rise to post-shock excitations away from the electrodes. Another mechanism for defibrillation success and failure of biphasic defibrillation uncovered by simulation studies is the formation of VEP-induced graded responses (below threshold depolarizations) following biphasic shocks:^{45,46} the development of a propagated activity following a graded response was found to result in a failure of a biphasic defibrillation shock and vice versa.

The isoelectric window

In the shock failure episodes with shock strengths significantly below the ULV or the DFT, arrhythmia is induced mostly right after the shock, initiated typically by a break excitation wave that reenters in the heart. However, numerous studies mapping the epicardium, mostly electrical^{47–54} but also some optical,^{55–57} have demonstrated

that following failed defibrillation shocks or shocks applied during the vulnerable period, the strength of which was close (but still below) the DFT or ULV, reentrant patterns were not always immediately observed (on the epicardium). Although some local epicardial activations were detected in these cases, these activations did not become global and quickly died,^{58–61} followed by an electrically quiescent period on the epicardium termed the 'isoelectric window'. The mechanisms underlying the origin of the first global post-shock activations following the isoelectric window have also been the topic of much discussion and debate. Understanding the mechanisms responsible for the formation of an isoelectric window on the ventricular surface and the origins of the post-shock activations following it is of great importance for uncovering the mechanisms of defibrillation failure.

A recent 3D simulation study proposed a new mechanism for the existence of the isoelectric window.¹ Figure 2, top, presents an episode of earliest post-shock activation following an isoelectric window in a 16 V/cm monophasic shock. Formation of VEP, quick re-excitation, and synchronous repolarization take place sequentially. However, a wavefront which originated at a location deep within the wall remained submerged (transparent panel, wavefront indicated by *) until it made a breakthrough onto the epicardium and then propagated, resulting in intramural reentry. In this example, the isoelectric window was nearly 80 ms. Figure 2, bottom, presents an example of a post-shock activation following an isoelectric

window induced by a 12 V/cm biphasic shock. Here again, the wavefront originating 20 ms after shock-end (* in transparent view), which remained submerged for another 35 ms, made a breakthrough onto the epicardium, resulting in an intramural scroll wave. In this case the isoelectric window was ~55 ms.

The existence of the isoelectric window on the epicardium is explained by the presence of intramural excitable areas and propagation of the post-shock activations through these areas deep in the ventricular wall and away from the surfaces ('tunnel propagation'). These intramural wavefronts cannot make a breakthrough on the ventricular surface because of the long-lasting post-shock depolarization of the surfaces. Only when the surfaces recover from this depolarization, the intramural wavefronts propagating in the mid-wall tunnel are able to make a breakthrough on the wall surface, marking the end of the isoelectric window. Such intramural post-shock propagation is consistent with transmural plunge electrode recordings, demonstrating that the site of origin of the post-shock activation was within the myocardium rather than on the surface.^{47,54}

In an article by Constantino *et al.*,⁵ the new theory of tunnel propagation for near-ULV/DFT shocks was extended to explain the mechanisms responsible for the existence of isoelectric window following implantable cardioverter-defibrillator (ICD) shocks delivered to the fibrillating heart. The simulation results demonstrated that the non-uniform field created by ICD electrodes, combined with the fibre

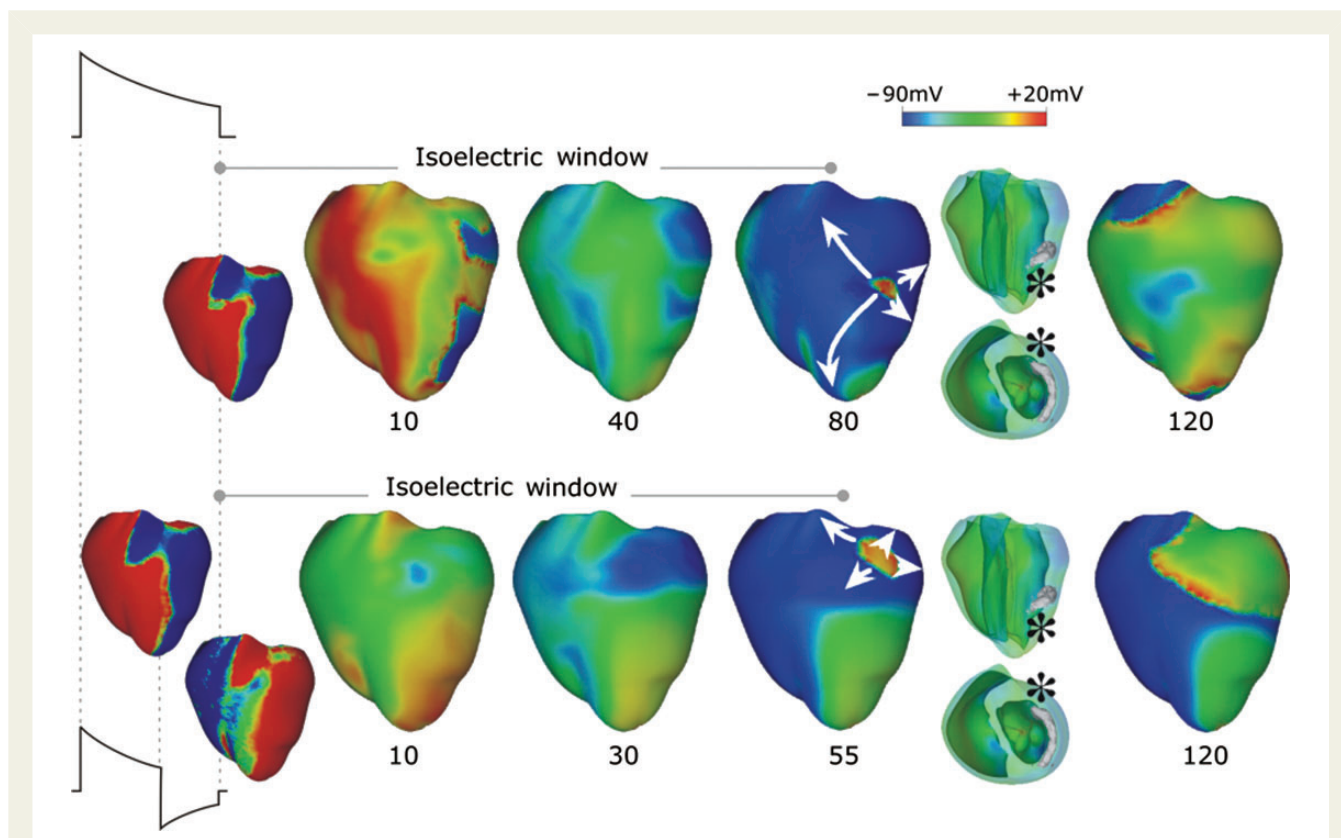


Figure 2 Monophasic (top) and biphasic (bottom) shock episodes resulting in isoelectric window and arrhythmia initiation. Progression of activity from VEP through initiation of intramural activation (transparent view with activation marked by *) to epicardial breakthrough followed by focal activation pattern and ultimately a reentry. Shocks are external of duration 10 ms (6/4 ms for the biphasic shock) and of strengths 16 (monophasic) and 12 (biphasic) V/cm and are delivered at 220 ms coupling interval. Images based on figures published in Ashihara *et al.*¹

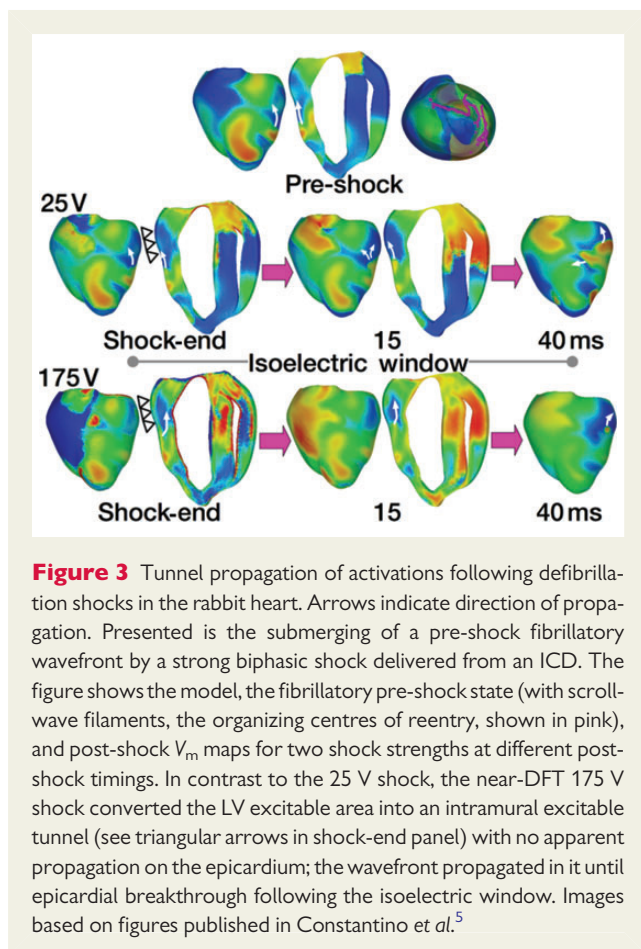


Figure 3 Tunnel propagation of activations following defibrillation shocks in the rabbit heart. Arrows indicate direction of propagation. Presented is the submerging of a pre-shock fibrillatory wavefront by a strong biphasic shock delivered from an ICD. The figure shows the model, the fibrillatory pre-shock state (with scroll-wave filaments, the organizing centres of reentry, shown in pink), and post-shock V_m maps for two shock strengths at different post-shock timings. In contrast to the 25 V shock, the near-DFT 175 V shock converted the LV excitable area into an intramural excitable tunnel (see triangular arrows in shock-end panel) with no apparent propagation on the epicardium; the wavefront propagated in it until epicardial breakthrough following the isoelectric window. Images based on figures published in Constantino *et al.*⁵

orientation and complex geometry of the ventricles, resulted in a post-shock excitable region located always in the left ventricular (LV) free wall, regardless of pre-shock state. For near-ULV/DFT shocks, this excitable region was converted into an intramural tunnel (Figure 3), through which either pre-existing fibrillatory or shock-induced wavefronts propagated during the isoelectric window, emerging as breakthroughs on the LV epicardium. Interestingly, failed defibrillation for near-DFT shocks was found to not always be associated with termination of existing wavefronts and generation of new wavefronts by the shock, as previously believed; instead, the wavefronts remained ‘alive’ in the intramural post-shock tunnel. Pre-shock activity within the LV played a significant role in shock outcome: a large number of pre-shock fibrillatory wavefronts resulted in an isoelectric window associated with tunnel propagation of pre-existing rather than shock-induced wavefronts. Furthermore, shocks were more likely to succeed if the LV excitable area was smaller.

A schematic¹⁵ of the mechanisms of defibrillation failure for shocks well below the DFT and near it is presented in Figure 4.

Computational modelling of defibrillation in the ischaemic and infarcted heart

The quest to unravel how shocks succeed in terminating fibrillation or re-initiate arrhythmia, as described above, commenced with

studies in the normal heart. However, the majority of patients who receive defibrillation shocks have an underlying cardiac disease. In the section below, we present simulation research on defibrillation mechanisms in the ischaemic and infarcted heart.

The ischaemic heart

Two studies by Rodriguez *et al.*^{62,63} characterized the changes in vulnerability to electric shocks during phase 1A of global ischaemia and determined the mechanisms responsible for these changes. These studies focused on global ischaemia as an important step in understanding the mechanisms that underlie vulnerability to electric shocks following an ischaemic event associated with coronary heart disease. The studies used a 3D bidomain model, first of a slice of the canine heart, and then of the ischaemic rabbit ventricles. Global ischaemia was implemented by representing changes in membrane dynamics over the course of the first 10 min following coronary occlusion. Progression of ischaemia phase 1A was represented by linear changes in remodelled ionic currents. To study vulnerability to shocks, three representative ischaemic levels of increasing severity within this 10 min interval were chosen.

To examine vulnerability to arrhythmia, monophasic shocks were applied to the models at various coupling intervals to construct vulnerability grids in normoxia and at various stages of ischaemia phase 1A. The simulations demonstrated that 2–3 min after the onset of ischaemia, the ULV remained at its normoxic value, although arrhythmias are induced at shorter coupling intervals. As ischaemia progressed, the ULV decreased, and the vulnerable window shifted towards longer coupling intervals. Altogether, the ventricles become less vulnerable to electric shocks as global ischaemia phase 1A progressed. Dissecting out the mechanisms responsible for this behaviour revealed that the changes in the ULV resulted from an increase in the spatial extent of the excitation wavefronts arising at shock-end, and the slower recovery from shock-induced positive polarization. The shifts in the vulnerable window were found to stem from decreases in local repolarization times and the occurrence of post-shock conduction failure caused by prolonged post-repolarization refractoriness.

The infarcted heart

Defibrillation efficacy is decreased in infarcted hearts, but the mechanisms by which infarcted hearts are more vulnerable to electric shocks than healthy hearts remain poorly understood. The study by Rantner *et al.*⁶ provided insight into the 3D mechanisms for the increased vulnerability to electric shocks in infarcted hearts. This study developed a microanatomically detailed rabbit ventricular model with chronic myocardial infarction from magnetic resonance imaging (MRI) and diffusion tensor MRI scans (Figures 5A and B); the model was further enriched with data from optical mapping experiments. The infarct incorporated an infarct scar (inexcitable) and a partially viable peri-infarct zone (PZ); the latter has been shown to dramatically increase the propensity to arrhythmia.⁶⁴

The simulation protocol involved apical pacing followed by biphasic shocks. Simulation results were compared with those using the same rabbit ventricular model but without the infarct. The ULV was significantly increased in infarction – 8 V/cm in the infarction model vs. 4 V/cm in the control model. Analysis of the simulation results revealed that VEPs were less pronounced in the infarction

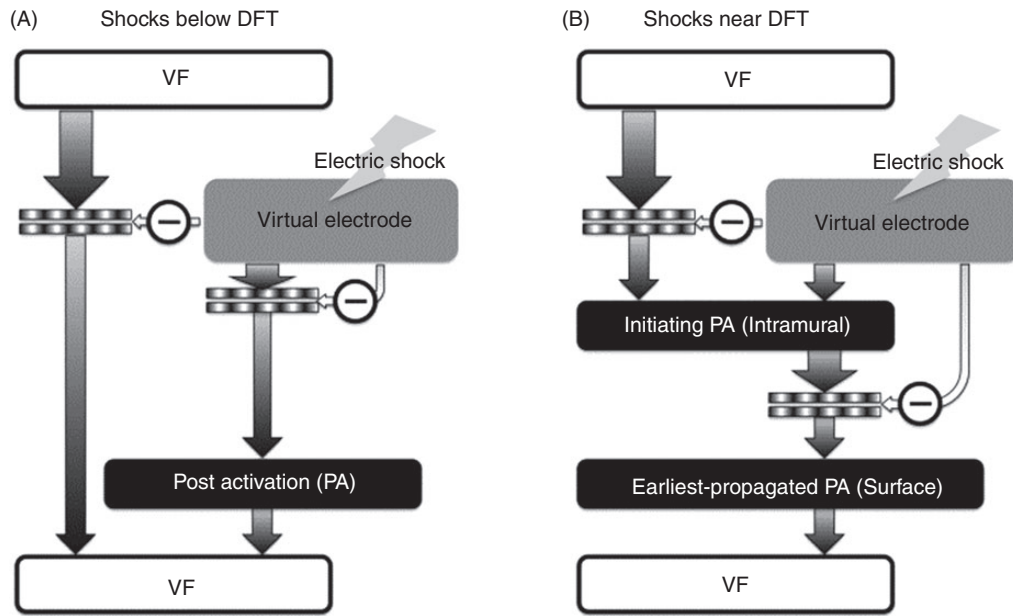


Figure 4 Mechanisms for shock failure, for shocks far below (A) and near (B) the DFT. In (A), arrhythmia is induced right after the shock, initiated by a post-shock activation (typically a break excitation wave) that reenters in the heart. In (B), the presence of only intramural excitable areas results in propagation of post-shock activations initiated in these areas deep in the ventricular wall ("tunnel propagation"). These intramural wavefronts cannot make a breakthrough on the ventricular surface because of the post-shock depolarization of the surfaces. Only when the surfaces recover from this depolarization, the intramural wavefronts propagating in the mid-wall tunnel are able to make a breakthrough on the wall surfaces, marking the end of the isoelectric window, and becoming the earliest propagated post-shock activations propagating globally (and thus on the ventricular surfaces). Image based on figure published in Trayanova *et al.*¹⁵

model. Figure 5C shows the depolarizing (virtual cathodes; red areas) and hyperpolarizing (virtual anodes; blue areas) membrane effects of the electric shock. The small panel on the far right shows the differences in VEP between infarction and control (as control minus infarction). It is evident from the figure that VEPs were less positive in infarction than in control in the PZ and on the LV endocardium; on average, there was stronger shock-induced depolarization in the healthy tissue than in the PZ. Mechanistically, the altered distribution of VEP in the infarction model provided a larger excitable area for post-shock propagation but smaller V_m gradients to initiate new wavefronts. Initial post-shock transmural activation therefore occurred at a later time in the infarction model, and the remodelled ionic properties in the PZ served to delay propagation in subsequent beats, increasing vulnerability to electric shocks in the infarcted heart.

Simulations of novel defibrillation modalities: high-frequency and low-voltage defibrillation

In the last couple of years, defibrillation modelling has focused on the development of new methodologies for low-voltage termination of lethal arrhythmias or for applying defibrillation in novel, less damaging ways. A recent novel approach to defibrillation was presented by Tandri *et al.*,⁶⁵ based on the premise that sustained kilohertz-range

alternating current (AC) fields have been known to instantaneously and reversibly block electrical conduction in nerve tissue. The article provided proof of the concept that electric fields, such as those used for neural block, when applied to cardiac tissue, similarly produce reversible block of cardiac impulse propagation and lead to successful defibrillation, and that this methodology could potentially be a safer means for terminating life-threatening reentrant arrhythmias. Understanding the mechanisms of this new mode of defibrillation relied also on biophysically detailed modelling of heart electrophysiology.⁶⁶ The data revealed a previously unrecognized capacity for myocardial cells to be placed in an extended but immediately reversible state of refractoriness by an applied electric field. The imposed refractory state blocked all wave propagation and resulted in termination of reentrant arrhythmias, without impairment of subsequent cellular electrical function or initiation of post-shock fibrillatory activity. Since the same AC fields block neural and cardiac activity equally well, the proposed defibrillation methodology could possibly be utilized to achieve high voltage, yet painless defibrillation.

Recent experimental studies have shown that applied electric fields delivering multiple far-field stimuli at a given cycle length can terminate ventricular tachycardia (VT), atrial flutter, and atrial fibrillation with less total energy than a single strong shock.^{67–70} However, the mechanisms and full range of applications of this new mode of defibrillation have remained poorly explored. The recent simulation study by

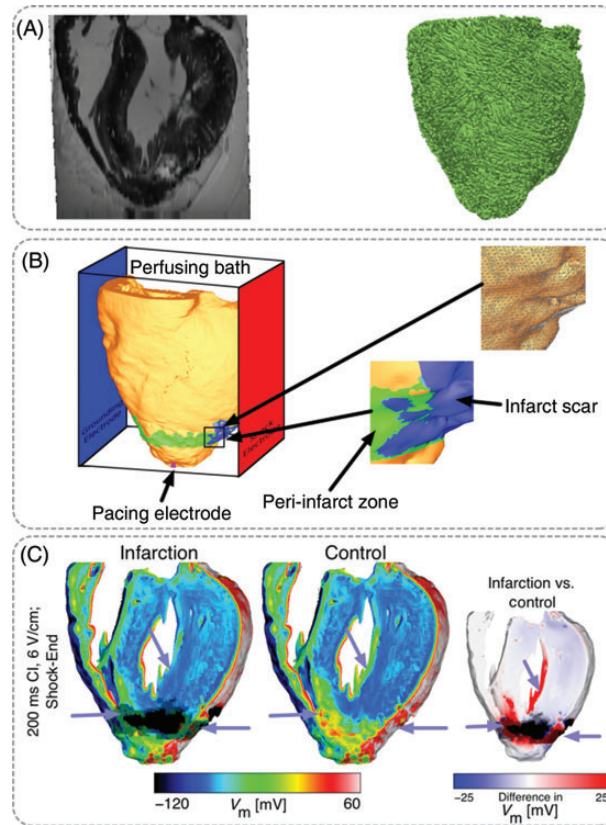


Figure 5 MRI-based model of healed infarction in the rabbit. (A) *Ex-vivo* MRI scan of the rabbit heart with healed myocardial infarction and anterior view of the fibre orientations in the ventricles. (B) Left panel, anterior view of the ventricles submerged in a perfusing bath and placed between plate electrodes (blue, grounding electrode; red, shock electrode). The infarct scar is shown in blue, the peri-infarct (border) zone is shown in green. The pink square at the apex shows the location of the pacing electrode. The bottom inset shows the highly detailed structure of the scar and the PZ. The top inset shows the details of the computational mesh. (C) Distribution of shock-end V_m . Less tissue was excited in the infarction model (purple arrows). Right-most panel shows the V_m difference between infarction and control models, computed as control V_m minus infarction V_m . Images based on figures published in Rantner *et al.*⁶



Figure 6 Implantable cardioverter-defibrillator configurations tested in the paediatric patient with tricuspid valve atresia. Figure modified with permission from Rantner *et al.*⁷²

Rantner *et al.*⁷¹ aimed to elucidate these mechanisms and to develop an optimal low-voltage defibrillation protocol. Based on the simulation results using a complex high-resolution MRI-based model, a novel

two-stage low-voltage defibrillation protocol was proposed that did not involve the delivery of the stimuli at a constant cycle length. Instead, the first stage converted VF into VT by applying low-voltage

stimuli at times of maximal excitable gap, capturing a large tissue volume and synchronizing depolarization. The second stage then terminated VT by multiple low-voltage stimuli given at constant cycle lengths. The energy required for successful defibrillation using this protocol was 57.42% of the energy for low-voltage defibrillation when stimulating at the optimal fixed-duration cycle length.

Towards clinical translation of defibrillation simulations

Finally, a recent study⁷² has made the first attempt towards clinical translation of computer models of defibrillation. The study made the first step towards addressing a clinical need: ICDs with transvenous leads often cannot be implanted in a standard manner in paediatric and congenital heart defect (CHD) patients; currently, there is no reliable approach to predict the optimal ICD placement in these patients. The study provided the proof-of-concept that patient-specific biophysically detailed computer simulations of the dynamic process of defibrillation could be used to predict the optimal location of the ICD leads in these patients. A pipeline for constructing personalized, electrophysiological heart–torso models from clinical MRI scans was developed and applied to a paediatric CHD patient, and the optimal ICD placement was determined using patient-specific simulations of defibrillation. *Figure 6* shows some of the different configurations tested. In a patient with tricuspid valve atresia, two configurations with epicardial leads were found to have the lowest DFT. The study demonstrated that using such methodology, the optimal ICD placement in paediatric/CHD patients could be predicted computationally, which could reduce defibrillation energy if the pipeline is used as part of ICD implantation planning.

Concluding remarks

The information and examples presented in this review regarding the insights provided by the 3D models of shock-induced arrhythmogenesis and defibrillation underscore the achievements and power of realistic modelling and simulation in uncovering and understanding cardiac electrophysiology phenomena. Simulations of defibrillation are particularly useful in revealing shock-induced electrical behaviour hidden within the cardiac wall; insights into vulnerability and defibrillation, such as these presented here, cannot be achieved with experimental methodology alone. Supported by experimental observations of behaviour during and after the shock over the cardiac surfaces, realistic whole-organ simulations have become invaluable in understanding the interaction of the applied electric field with the wavefronts of fibrillation; important insights have been generated by models representing the diseased heart. Defibrillation models are now being utilized to explore novel modalities for defibrillation, such as high frequency or low voltage. Importantly, initial steps have been made in the use of computer simulations to guide the implantation of ICDs in paediatric and congenital heart disease patients. In addition to defibrillation, biophysically detailed realistic-geometry heart models are currently being employed and are expected to successfully contribute to the study of many other aspects of the mechanisms of

arrhythmogenesis as well as to serve as a testbed for other potential anti-arrhythmia therapies.

Conflict of interest: N.A.T. has partial ownership of CardioSolv, LLC; CardioSolv, LLC was not involved in this research; L.J.R. has no conflict of interest to declare.

Funding

This work was supported by the National Institutes of Health (R01-HL103428 to N.A.T.).

References

- Ashihara T, Constantino J, Trayanova NA. Tunnel propagation of postshock activations as a hypothesis for fibrillation induction and isoelectric window. *Circ Res* 2008; **102**:737–45.
- Rodriguez B, Li L, Eason JC, Efimov IR, Trayanova NA. Differences between left and right ventricular chamber geometry affect cardiac vulnerability to electric shocks. *Circ Res* 2005; **97**:168–75.
- Arevalo H, Rodriguez B, Trayanova N. Arrhythmogenesis in the heart: multiscale modeling of the effects of defibrillation shocks and the role of electrophysiological heterogeneity. *Chaos* 2007; **17**:015103.
- Plank G, Prassl A, Hofer E, Trayanova NA. Evaluating intramural virtual electrodes in the myocardial wedge preparation: simulations of experimental conditions. *Biophys J* 2008; **94**:1904–15.
- Constantino J, Long Y, Ashihara T, Trayanova NA. Tunnel propagation following defibrillation with ICD shocks: hidden postshock activations in the left ventricular wall underlie isoelectric window. *Heart Rhythm* 2010; **7**:953–61.
- Rantner LJ, Arevalo HJ, Constantino JL, Efimov IR, Plank G, Trayanova NA. Three-dimensional mechanisms of increased vulnerability to electric shocks in myocardial infarction: altered virtual electrode polarizations and conduction delay in the perinfarct zone. *J Physiol* 2012; **590**:4537–51.
- Rantner LJ, Tice BM, Trayanova NA. Terminating ventricular tachyarrhythmias using far-field low-voltage stimuli: mechanisms and delivery protocols. *Heart Rhythm* 2013; **10**:1209–17.
- Aguel F, Campbell C, Trayanova NA. Active bidomain simulation of defibrillation in whole rabbit ventricles with real fiber orientation (abstract). *Ann Biomed Eng* 2001; **29**:S48.
- Efimov IR, Aguel F, Cheng Y, Wollenzier B, Trayanova N. Virtual electrode polarization in the far field: implications for external defibrillation. *Am J Physiol Heart Circ Physiol* 2000; **279**:H1055–70.
- Aguel F, Eason J, Trayanova N. Advances in modeling cardiac defibrillation. *Int J Bifurcation Chaos* 2003; **13**:3791–805.
- Maharaj T, Blake R, Trayanova N, Gavaghan D, Rodriguez B. The role of transmural ventricular heterogeneities in cardiac vulnerability to electric shocks. *Prog Biophys Mol Biol*. 2008; **96**:321–38.
- Trayanova N, Eason J, Aguel F. Computer simulations of cardiac defibrillation: a look inside the heart. *Comput Vis Sci* 2002; **4**:259–70.
- Bishop MJ, Rodriguez B, Qu F, Efimov IR, Gavaghan DJ, Trayanova NA. The role of photon scattering in optical signal distortion during arrhythmia and defibrillation. *Biophys J* 2007; **93**:3714–26.
- Sepulveda NG, Roth BJ, Wikswo JP Jr. Current injection into a two-dimensional anisotropic bidomain. *Biophys J* 1989; **55**:987–99.
- Trayanova N, Constantino J, Ashihara T, Plank G. Modeling defibrillation of the heart: approaches and insights. *IEEE Rev Biomed Eng* 2011; **4**:89–102.
- Wikswo JP Jr, Lin SF, Abbas RA. Virtual electrodes in cardiac tissue: a common mechanism for anodal and cathodal stimulation. *Biophys J* 1995; **69**:2195–210.
- Efimov IR, Cheng YN, Biermann M, Van Wagoner DR, Mazgalev TN, Tchou PJ. Transmembrane voltage changes produced by real and virtual electrodes during monophasic defibrillation shock delivered by an implantable electrode. *J Cardiovasc Electrophysiol* 1997; **8**:1031–45.
- Knisley SB, Trayanova N, Aguel F. Roles of electric field and fiber structure in cardiac electric stimulation. *Biophys J* 1999; **77**:1404–17.
- Efimov IR, Gray RA, Roth BJ. Virtual electrodes and deexcitation: new insights into fibrillation induction and defibrillation. *J Cardiovasc Electrophysiol* 2000; **11**:339–53.
- Lindblom AE, Roth BJ, Trayanova NA. Role of virtual electrodes in arrhythmogenesis: pinwheel experiment revisited. *J Cardiovasc Electrophysiol* 2000; **11**:274–85.
- Lindblom AE, Aguel F, Trayanova NA. Virtual electrode polarization leads to reentry in the far field. *J Cardiovasc Electrophysiol* 2001; **12**:946–56.

22. Trayanova NA, Eason JC, Anderson C, Aguel F. Computer modeling of defibrillation ii: why does the shock fail? In Cabo C, Rosenbaum D, (eds). *Quantitative cardiac electrophysiology*. New York: Marcel Dekker; 2002. p. 220–243.
23. Trayanova NA, Eason J. Shock-induced arrhythmogenesis in the myocardium. *Chaos* 2002;**359**:1327–37.
24. Sobie EA, Susil RC, Tung L. A generalized activating function for predicting virtual electrodes in cardiac tissue. *Biophys J* 1997;**73**:1410–23.
25. Trayanova NA. Far-field stimulation of cardiac tissue. *Herzschrittmacherther Electro-physiol* 1999;**10**:137–48.
26. Trayanova NA. Concepts of defibrillation. *Phil Trans R Soc London A* 2001;**359**:1327–37.
27. Trayanova N, Skouibine K, Aguel F. The role of cardiac tissue structure in defibrillation. *Chaos* 1998;**8**:221–33.
28. Entcheva E, Trayanova NA, Claydon FJ. Patterns of and mechanisms for shock-induced polarization in the heart: a bidomain analysis. *IEEE Trans Biomed Eng* 1999;**46**:260–70.
29. Trayanova NA, Roth BJ, Malden LJ. The response of a spherical heart to a uniform electric field: a bidomain analysis of cardiac stimulation. *IEEE Trans Biomed Eng* 1993;**40**:899–908.
30. Fast VG, Rohr S, Gillis AM, Kleber AG. Activation of cardiac tissue by extracellular electrical shocks: formation of 'secondary sources' at intercellular clefts in monolayers of cultured myocytes. *Circ Res* 1998;**82**:375–85.
31. Fishler MG. Syncytial heterogeneity as a mechanism underlying cardiac far-field stimulation during defibrillation-level shocks. *J Cardiovasc Electrophysiol* 1998;**9**:384–94.
32. Hooks DA, Tomlinson KA, Marsden SG, LeGrice IJ, Small BH, Pullan AJ *et al*. Cardiac microstructure: implications for electrical propagation and defibrillation in the heart. *Circ Res* 2002;**91**:331–8.
33. Rodriguez B, Trayanova N. Upper limit of vulnerability in a defibrillation model of the rabbit ventricles. *J Electrocardiol* 2003;**36**(Suppl):51–6.
34. Roth BJ. A mathematical model of make and break electrical stimulation of cardiac tissue by a unipolar anode or cathode. *IEEE Trans Biomed Eng* 1995;**42**:1174–84.
35. Cheng Y, Mowrey KA, Van Wagoner DR, Tchou PJ, Efimov IR. Virtual electrode-induced reexcitation: a mechanism of defibrillation. *Circ Res* 1999;**85**:1056–66.
36. Maleckar MM, Woods MC, Sidorov VY, Holcomb MR, Mashburn DN, Wikswo JP *et al*. Polarity reversal lowers activation time during diastolic field stimulation of the rabbit ventricles: insights into mechanisms. *Am J Physiol Heart Circ Physiol* 2008;**295**:H1626–33.
37. Skouibine K, Trayanova N, Moore P. Success and failure of the defibrillation shock: insights from a simulation study. *J Cardiovasc Electrophysiol* 2000;**11**:785–96.
38. Knisley SB, Smith WM, Ideker RE. Prolongation and shortening of action potentials by electrical shocks in frog ventricular muscle. *Am J Physiol* 1994;**266**:H2348–58.
39. Hillebrenner MG, Eason JC, Campbell CA, Trayanova NA. Postshock arrhythmogenesis in a slice of the canine heart. *J Cardiovasc Electrophysiol* 2003;**14**:S249–56.
40. Hillebrenner MG, Eason JC, Trayanova NA. Mechanistic inquiry into decrease in probability of defibrillation success with increase in complexity of preshock reentrant activity. *Am J Physiol Heart Circ Physiol* 2004;**286**:H909–17.
41. Bishop M, Rodriguez B, Eason J, Whiteley J, Trayanova N, Gavaghan D. Synthesis of voltage-sensitive optical signals: application to panoramic optical mapping. *Biophys J* 2006;**90**:2938–45.
42. Chen P-S, Ideker RE, Smith WM, Danielely ND, Melnick SD, Wolf PD. Comparison of activation during ventricular fibrillation and following unsuccessful defibrillation shocks in open-chest dogs. *Circ Res* 1990;**66**:1544–60.
43. Chen P-S, Feld GK, Kriett JM, Mower MM, Tarazi RY, Fleck RP *et al*. Relation between upper limit of vulnerability and defibrillation threshold in humans. *Circulation* 1993;**88**:186–92.
44. Anderson C, Trayanova NA, Skouibine K. Termination of spiral waves with biphasic shocks: the role of virtual electrode polarization. *J Cardiovasc Electrophysiol* 2000;**11**:1386–96.
45. Trayanova NA, Gray RA, Bourn DW, Eason JC. Virtual electrode induced positive and negative graded responses: new insights into fibrillation induction in defibrillation. *J Cardiovasc Electrophysiol* 2003;**14**:756–63.
46. Bourn DW, Trayanova NA, Gray RA. Shock-induced arrhythmogenesis and isoelectric window. *Pacing Clin Electrophysiol* 2002;**25**:604.
47. Chen PS, Shibata N, Dixon EG, Wolf PD, Danielely ND, Sweeney MB *et al*. Activation during ventricular defibrillation in open-chest dogs. Evidence of complete cessation and regeneration of ventricular fibrillation after unsuccessful shocks. *J Clin Invest* 1986;**77**:810–23.
48. Chen P-S, Shibata N, Dixon EG, Martin RO, Ideker RE. Comparison of the defibrillation threshold and the upper limit of ventricular vulnerability. *Circulation* 1986;**73**:1022–8.
49. Shibata N, Chen PS, Dixon EG, Wolf PD, Danielely ND, Smith WM *et al*. Epicardial activation after unsuccessful defibrillation shocks in dogs. *Am J Physiol* 1988;**255**:H902–9.
50. Zhou X, Daubert JP, Wolf PD, Smith WM, Ideker RE. Epicardial mapping of ventricular defibrillation with monophasic and biphasic shocks in dogs. *Circ Res* 1993;**72**:145–60.
51. Usui M, Callihan RL, Walker RG, Walcott GP, Rollins DL, Wolf PD *et al*. Epicardial sock mapping following monophasic and biphasic shocks of equal voltage with an endocardial lead system. *J Cardiovasc Electrophysiol* 1996;**7**:322–34.
52. Chattapakorn N, Fotuhi PC, Ideker RE. Prediction of defibrillation outcome by epicardial activation patterns following shocks near the defibrillation threshold. *J Cardiovasc Electrophysiol* 2000;**11**:1014–21.
53. Chattapakorn N, Rogers J, Ideker RE. Influence of postshock epicardial activation patterns on initiation of ventricular fibrillation by upper limit of vulnerability shocks. *Circulation* 2000;**101**:1329–36.
54. Chattapakorn N, Fotuhi PC, Chattapakorn SC, Ideker RE. Three-dimensional mapping of earliest activation after near-threshold ventricular defibrillation shocks. *J Cardiovasc Electrophysiol* 2003;**14**:65–9.
55. Chattapakorn N, Banville I, Gray RA, Ideker RE. Mechanism of ventricular defibrillation for near-defibrillation threshold shocks: a whole-heart optical mapping study in swine. *Circulation* 2001;**104**:1515–25.
56. Wang NC, Lee M-H, Ohara T, Okuyama Y, Fishbein GA, Lin S-F *et al*. Optical mapping of ventricular defibrillation in isolated swine ventricles: demonstration of a post-shock isoelectric window after near-threshold defibrillation shocks. *Circulation* 2001;**104**:227–33.
57. Chattapakorn N, Banville I, Gray RA, Ideker RE. Effects of shock strengths on ventricular defibrillation failure. *Cardiovasc Res* 2004;**61**:39–44.
58. Moe GK, Harris AS, Wiggers CJ. Analysis of the initiation of fibrillation by electrographic studies. *Am J Physiol* 1941;**134**:473–92.
59. Shibata N, Chen PS, Dixon EG, Wolf PD, Danielely ND, Smith WM *et al*. Influence of shock strength and timing on induction of ventricular arrhythmias in dogs. *Am J Physiol* 1988;**255**:H891–901.
60. Idriss SF, Wolf PD, Smith WM, Ideker RE. Effect of pacing site on ventricular fibrillation initiation by shocks during the vulnerable period. *Am J Physiol* 1999;**277**:H2065–82.
61. Chattapakorn N, KenKnight BH, Rogers JM, Walker RG, Walcott GP, Rollins DL *et al*. Locally propagated activation immediately after internal defibrillation. *Circulation* 1998;**97**:1401–10.
62. Rodriguez B, Tice BM, Eason JC, Aguel F, Ferrero JM Jr, Trayanova N. Effect of acute global ischemia on the upper limit of vulnerability: a simulation study. *Am J Physiol Heart Circ Physiol* 2004;**286**:H2078–88.
63. Rodriguez B, Tice B, Eason J, Aguel F, Trayanova N. Cardiac vulnerability to electric shocks during phase 1a of acute global ischemia. *Heart Rhythm* 2004;**6**:695–703.
64. Ashikaga H, Arevalo H, Vadakkumpadan F, Blake RC III, Bayer JD, Nazarian S *et al*. Feasibility of image-based simulation to estimate ablation target in human ventricular arrhythmia. *Heart Rhythm* 2013;**10**:1109–16.
65. Tandri H, Weinberg SH, Chang KC, Zhu R, Trayanova NA, Tung L *et al*. Reversible cardiac conduction block and defibrillation with high-frequency electric field. *Sci Transl Med* 2011;**3**:102ra196.
66. Weinberg SH, Chang KC, Zhu R, Tandri H, Berger RD, Trayanova NA *et al*. Defibrillation success with high frequency electric fields is related to degree and location of conduction block. *Heart Rhythm* 2013;**10**:740–8.
67. Fenton FH, Luther S, Cherry EM, Otani NF, Krinsky V, Pumir A *et al*. Termination of atrial fibrillation using pulsed low-energy far-field stimulation. *Circulation* 2009;**120**:467–76.
68. Luther S, Fenton FH, Kornreich BG, Squires A, Bittihn P, Hornung D *et al*. Low-energy control of electrical turbulence in the heart. *Nature* 2011;**475**:235–9.
69. Li W, Janardhan AH, Fedorov VV, Sha Q, Schuessler RB, Efimov IR. Low-energy multistage atrial defibrillation therapy terminates atrial fibrillation with less energy than a single shock. *Circ Arrhythm Electrophysiol* 2011;**4**:917–25.
70. Li W, Ripplinger CM, Lou Q, Efimov IR. Multiple monophasic shocks improve electrotherapy of ventricular tachycardia in a rabbit model of chronic infarction. *Heart Rhythm* 2009;**6**:1020–7.
71. Rantner LJ, Tice BM, Trayanova NA. Terminating ventricular tachyarrhythmias using far-field low-voltage stimuli: mechanisms and delivery protocols. *Heart Rhythm* 2013;**10**:1209–17.
72. Rantner LJ, Vadakkumpadan F, Spevak PJ, Crosson JE, Trayanova NA. Placement of implantable cardioverter-defibrillators in paediatric and congenital heart defect patients: a pipeline for model generation and simulation prediction of optimal configurations. *J Physiol* 2013;**591**:4321–34.